Dyes and Pigments 164 (2019) 62–71

Contents lists available at ScienceDirect

Dyes and Pigments

journal homepage: www.elsevier.com/locate/dyepig

Effect of mono alkoxy-carboxylate-functionalized benzothiadiazole-based donor polymers for non-fullerene solar cells

Gururaj P. Kini, Jun Young Choi, Sung Jae Jeon, Il Soon Suh, Doo Kyung Moon*

Nano and Information Materials (NIMs) Laboratory, Department of Chemical Engineering, Konkuk University, 120, Neungdong-ro, Gwangjin-gu, Seoul 05029, South Korea

ARTICLE INFO

Keywords:
Polymer solar cells
Benzothiadiazole
Carboxylate substituted benzothiadiazole
Carboxylate effect
Non-fullerene solar cells

ABSTRACT

Structural modification of benzo[c]-1,2,5-thiadiazole (BT) has been proved to be the prominent way to fine-tune the frontier energy levels and the intermolecular and intramolecular interactions in organic conjugated materials. In this study, a new acceptor unit, alkyl benzo[c][1,2,5]thiadiazole-5-carboxylate (BT-Est), was designed and synthesized by drafting mono alkoxy-carboxylate substituent on 5-position of BT core. Its compatibility in the conjugated system was investigated by co-polymerizing BT-Est with well-known benzo[1,2-*b*:4,5-*b*']dithiophene monomers containing either 2-(2-ethylhexyl)thienyl or 2-((2-ethylhexyl)thio)thienyl side chains to form two new polymers, **P1** and **P2**, respectively. The BT-Est yielded polymers with good solubility, medium bandgap (~1.71 eV), and deep highest occupied molecular orbital energy levels (−5.48 to −5.54 eV). Among the polymers, **P1** exhibited broader absorption, compact molecular packing, high charge carrier mobility, and effective exciton dissociation, despite of the torsion angle caused by the free rotation of the carboxylate group in the polymer backbone. Consequently, the best power-conversion efficiency of 6.9%, with a J_{SC} of 14.6 mA cm^{-2}, V_{OC} of 0.9 V, and FF of 52.5% were obtained for **P1**-based devices with the well-known non-fullerene acceptor ITIC. We systematically expounded the structure-property relationship of the BT-Est polymers using diverse characterization methods. Our results demonstrated that the mono carboxylate-substitution on the BT core can be used as the alternate strategy to modulate the optoelectronic properties and control the aggregation in the conjugated polymers. Thus, BT-Est has the potential to produce new donor–acceptor conjugated polymers and small molecules for application in organic electronics.

1. Introduction

Benzo[*c*]-1,2,5-thiadiazole (BT) [1–4] and its heteroannulated modifications like benzobisthiadiazole (BBT) [5–7], naphthobisthiadiazole (NTz) [8–11], dithieno[3′,2′:3,4; 2″,3″:5,6]benzo[1,2-*c*][1,2,5]thiadiazole (fDTBT) [12–14] have emerged as prominent electron-deficient acceptor cores for synthesizing donor–acceptor (D–A) polymers and small molecules for application in organic electronics. The chemical structure of BT has a strong electron-withdrawing 1,2,5-thiadiazole core attached to a benzene ring, allowing easy electron delocalization via *o*-benzoquinoidal nature, and thus lowering the energy bandgap and favoring ordered intermolecular packing [15]. The optoelectronic properties (energy levels, bandgap, etc.) of BT-based polymers can be easily tuned via functionalization of a 5,6-positions of the BT with either electron-deficient [1,2,16–25] or -donating [26–29] functional groups. Usually, the introduction of an electron-deficient heteroatom on BT will lower the frontier energy levels and influences the intramolecular and intermolecular interactions in the D–A polymers, thereby promoting effective charge transport [1,2,4,18–22]. Particularly, the incorporation of an fluorine or chlorine atoms on BT unit has attracted significant attention in recent years since it yields deep highest occupied molecular orbitals (HOMO), large dipole moments, good photostability, and impressive performances of the resultant polymers in polymer solar cells (PSCs) [4,16,18–20,23–25]. Despite the high power-conversion efficiencies (PCEs) obtained using these halogenated BT derivatives, their high aggregation tendencies, limited solubility and the use of hazardous halogenating reagents hinder their use as the active layer material in large-area roll-to-roll applications, where large quantities of raw materials required [4,20,30]. Therefore, it has become necessary to look for alternative techniques to overcome these drawbacks.

Nowadays, conjugated polymers having electron withdrawing carboxylate or ester (−COOR) substituents have demonstrated an impressive photovoltaic result over 10%, indicating their promising

* Corresponding author.
E-mail address: dkmoon@konkuk.ac.kr (D.K. Moon).

https://doi.org/10.1016/j.dyepig.2018.12.058
Received 9 November 2018; Received in revised form 5 December 2018; Accepted 26 December 2018
Available online 26 December 2018
0143-7208/

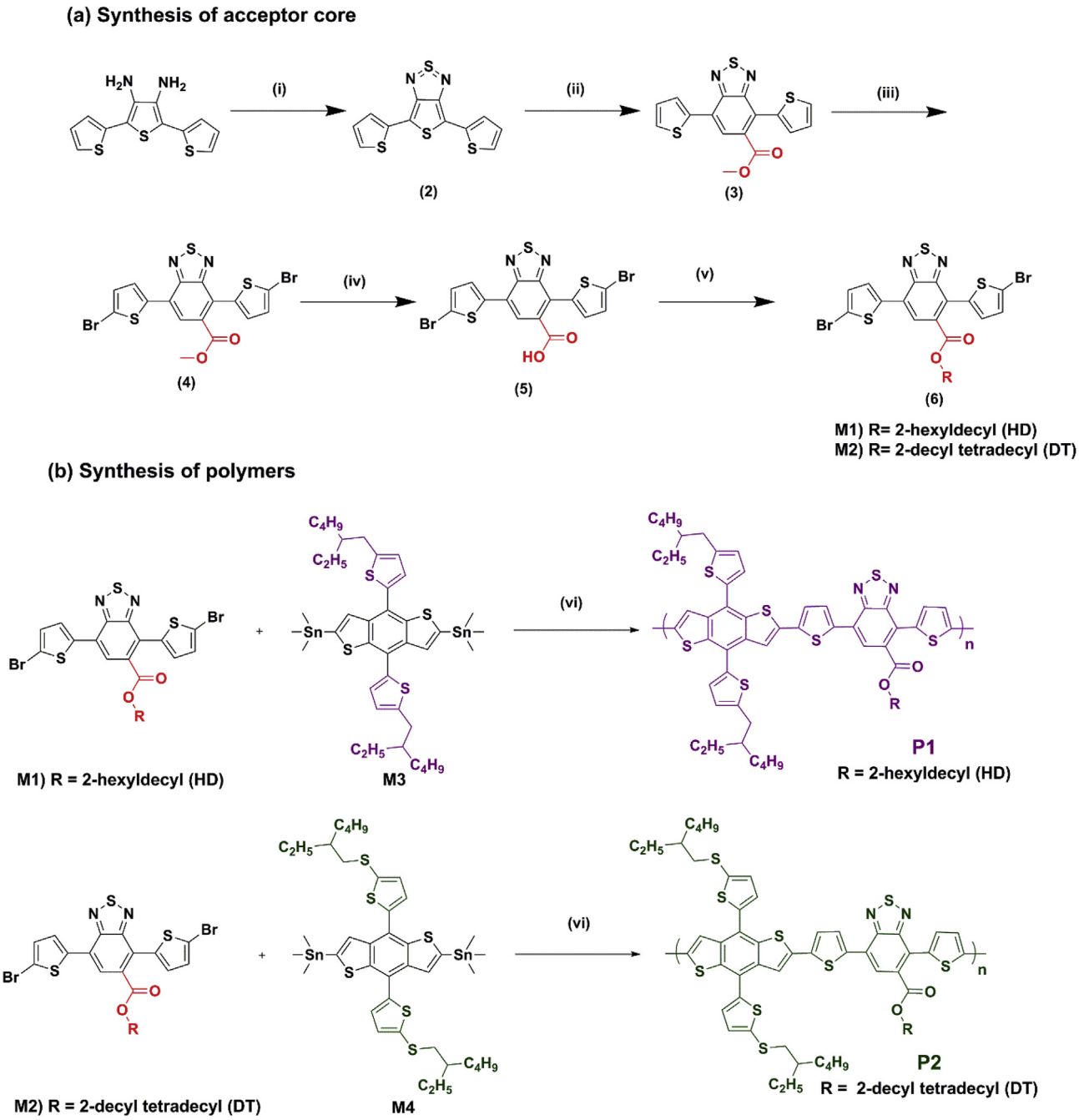

Scheme 1. Synthesis routes for BT-Est acceptor and polymers: (i) thionyl aniline, chlorotrimethyl silane, pyridine, RT, 3 h (90%); (ii) methyl propiolate, toluene, reflux, 36 h (70%); (iii) NBS, THF, RT, 16 h (64%); (iv) LiOH, MeOH–THF (1:1), reflux, 16 h (74%); (v) alcohol, DCC, DMAP, RT, 24 h (80–85%); (vi) $Pd_2(dba)_3$, tris (*o*-tolyl)phosphine, chlorobenzene, microwave (74–77%).

potential for application in PSCs [31–36]. These reports emphasize that the insertion of ester groups onto the conjugated polymer backbone have various advantages such as (1) easy tuning of solubility through alkyl chain modifications; (2) lower HOMO energy levels due to the higher electron-withdrawing ability; (3) enhanced planarity and crystallinity due to non-covalent interchain interactions; (4) good stability under continuous light illumination conditions [31–36]. However, there are only limited studies which emphasize the detailed opto-electronic properties of the carboxylate substituted BT polymers have been reported. This is due to the free rotation of the carboxylate group, which can negatively affect absorption and molecular packing in the conjugated backbone [37]. Recently, controlling number of substituents on the acceptor units is considered as one of the effective methods to overcome the planarity issues arising from the insertion of the substituents with the larger size [17–20,38]. For instance, Hu et al. substituted the different number of chlorine (Cl) atom on BT core with an aim of fine-tuning energy levels and aggregation in the resulted polymers [18]. Interestingly, the authors observed superior PCE of 8.21% for mono-Cl substituted polymer i.e. PCBT4T-2OD, which is approximately 34% higher than two-Cl counterpart (PCE of 6.12%). This enhancement of PCE is stemmed in from the increase in short-circuit current density (J_{SC}) and fill factor (FF), which was ascribed mainly due to the favorable molecular orientation, larger crystallite sizes and superior morphology showed by PCBT4T-2OD:$PC_{71}BM$ blends. In another case, He and co-workers achieved impressive PCEs up to 9.11% with the same acceptor, despite of large torsion angle in the backbone

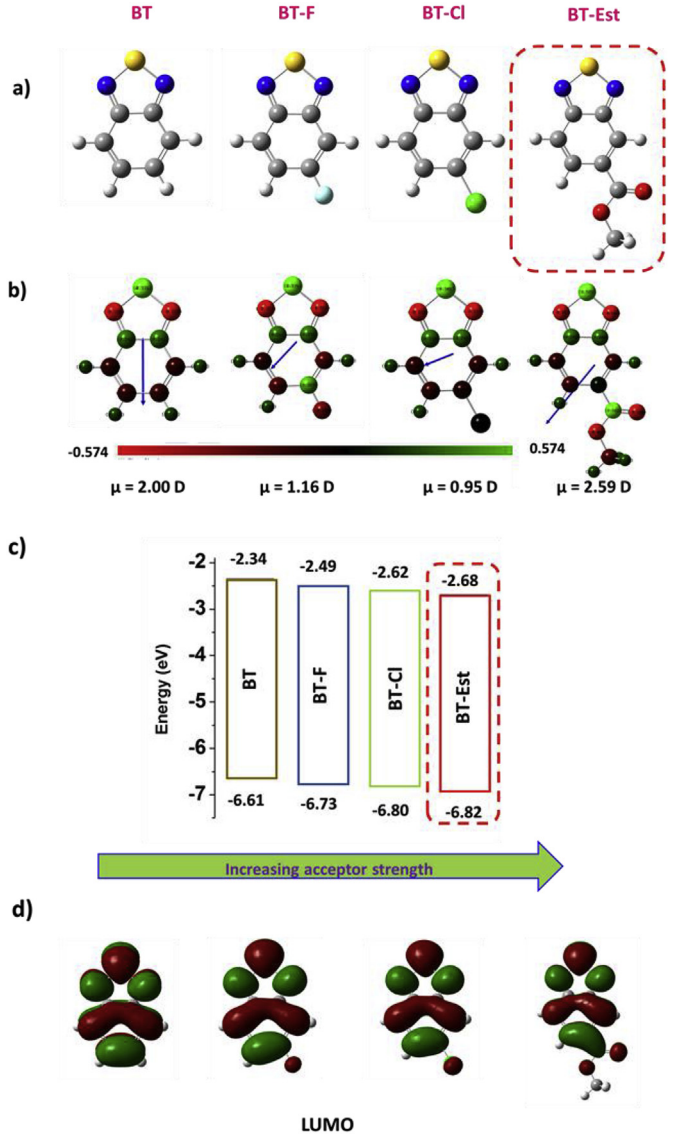

Fig. 1. Examples of chemical modification of the 2,1,3-benzothiadiazole (BT) system at the 5-position: (a) chemical structures; (b) direction and magnitude of the dipole moment; (c) theoretical HOMO and LUMO energy levels; and (d) spatial LUMO distributions (all data obtained using Gaussian 09 at the B3LYP/6–31G* level).

induced from the inserting Cl atom [19]. Likewise, Zhang et al. synthesized mono-chlorinated quinoxaline-based copolymer (Cl-PBTQT) based on a similar principle, which showed PCE of 8.16% [20]. These results clearly suggest that the higher performance can be achieved even with polymers having a non-planar conjugated backbone, unless the insertion of substituents with the larger size is not negatively affecting molecular packing in blend films.

In this report, we synthesized the new acceptor unit namely benzo[*c*][1,2,5]thiadiazole-5-carboxylate (BT-Est) by incorporating mono carboxylate group at the 5-position of dithienyl-flanked BT core, with a goal of achieving lower HOMO energy levels and easy tuning of solubility in the resulted polymers (Scheme 1). To check the compatibility of BT-Est, theoretical calculations were first performed using density functional theory (DFT) at the B3LYP/6-31G (d) level from the program Gaussian 09. The detailed comparison of the optimized molecular geometries, direction and magnitude of the dipole moment and HOMO and lowest unoccupied molecular orbital (LUMO) levels of newly synthesized BT-Est and previously reported BT derivatives such as 5-fluorobenzo[*c*][1,2,5]thiadiazole (BT-F), and 5-chlorobenzo[*c*][1,2,5] thiadiazole (BT-Cl) are shown in Fig. 1 and Table S1. Interestingly, BT-Est showed not only deeper HOMO and LUMO levels, but also higher dipole moment than BT, BT-F, and BT-Cl (Fig. 1b and c). This indicates that carboxylate substitution yields a stronger acceptor unit than either F or Cl substitution. Moreover, higher dipole moments can further aid self-assembly and charge separation in PSCs [39–41]. Notably, all BT derivatives exhibited similar electronic distributions (Fig. 1d), signifying that carboxylate functionalization has a minor effect on molecular orbital distributions. Therefore, BT-Est acceptor unit can be utilized for synthesizing D–A copolymers having low-lying frontier energy levels and good solubility.

Herein, we report the synthesis of BT-Est via mono-carboxylation of BT. To explore the compatibility of this acceptor in conjugated systems, we polymerized BT-Est with two well-known benzodithiophene donor monomers, 2-ethylhexylthienylbenzodithiophene and 2-ethylhexylthiothienylbenzodithiophene to obtain two new medium bandgap polymers, poly-{2-hexyldecyl 7-(5-(4,8-bis(5-(2-ethylhexyl)thiophen-2-yl)benzo[1,2-*b*:4,5-*b*']dithiophen-2-yl)thiophen-2-yl)-4-(thiophen-2-yl) benzo[*c*][1,2,5]thiadiazole-5-carboxylate} (**P1**) and poly-{2-decyltetradecyl 7-(5-(4,8-bis(5-((2-ethylhexyl)thio)thiophen-2-yl)benzo[1,2-*b*:4,5-*b*']dithiophen-2-yl)thiophen-2-yl)-4-(thiophen-2-yl)benzo[*c*] [1,2,5]thiadiazole-5-carboxylate (**P2**). We systematically evaluated the structure-property relationship between new acceptor in the conjugated system in detail by analysing and comparing DFT calculations, optical-electrochemical analysis, molecular ordering, and nanoscale film morphologies in the resultant D–A polymers as below.

2. Results and discussion

The synthesis of the BT-Est monomers and the polymers are shown in Scheme 1. The key electron-deficient intermediate (**2**) [42] and the benzodithiophene (BDT) monomers (**M3** and **M4**) [43,44] were synthesized according to previously reported procedures. On the other hand, compound **3** was prepared via cyclo-addition between **2** and methyl propiolate in toluene at 110 °C for 36 h. Then, the bromination of compound **3** using *N*-bromosuccinimide (NBS) afforded compound **4**, which was directly converted to its acidic intermediate (**5**) via hydrolysis. Next, intermediate **5** was reacted with different alkyl alcohols,

Table 1
Thermal, optical, and electrochemical properties of the BT–Est polymers.

Polymer	M_n [kDa]/ PDI[a]	Thermal property	Optical properties					Electrochemical properties	
		T_d [°C][b]	λ_{max} [nm], solution	ε (10^4) [M^{-1} cm^{-1}][c]	λ_{max} [nm], thin film	λ_{onset} [nm], thin film	E_g^{opt} [eV][d]	HOMO [eV]	LUMO [eV][e]
P1	61.9/1.79	383	592	4.24	614	744	1.67	−5.48	−3.81
P2	45.6/2.13	334	581	3.40	596	724	1.71	−5.54	−3.83

[a] Number-average molecular weight determined by GPC.
[b] Decomposition temperature (T_d) was determined by TGA (with 5% weight loss).
[c] The molar extinction coefficient of polymers at 600 nm in CF solution.
[d] Estimated values from the UV–vis absorption edge of the thin film (E_g^{opt} = 1240/λ_{onset}, eV).

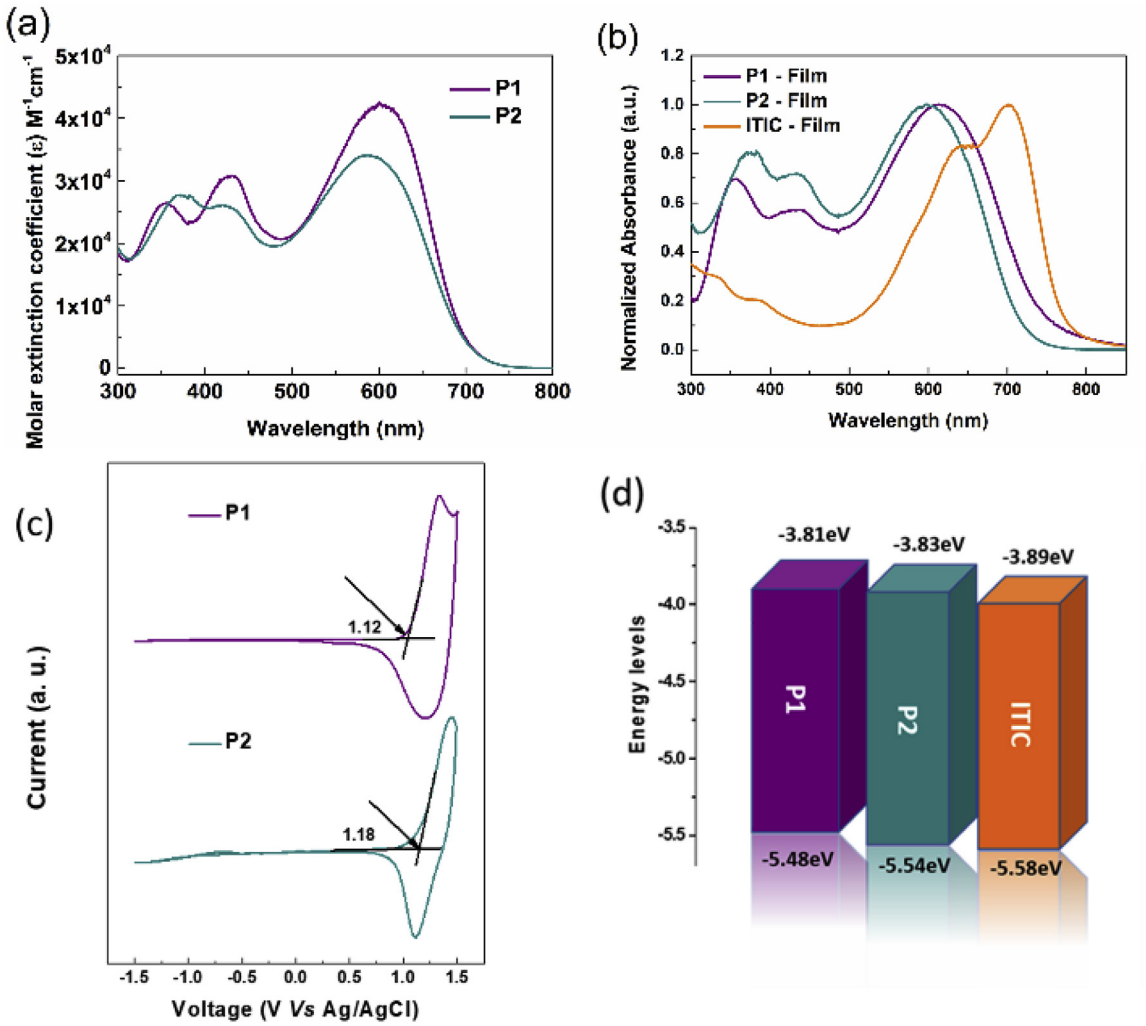

Fig. 2. Absorption spectra in (a) a chloroform (CF) solution and (b) the thin-film state, (c) cyclic voltammograms, and (d) energy levels of the BT-Est polymers.

using *N*,*N*′-dicyclohexylcarbodiimide (DCC) and 4-dimethylaminopyridine (DMAP) to produce the respective alkylated target monomers **M1** and **M2** with yields over 80%. Thus, BT-Est minimized the use of hazardous halogenated reagents and allowed direct tuning of the solubility by modifying alkyl side chains than halogenated BT derivatives. Finally, the polymers **P1** and **P2** were obtained by a typical Stille coupling reaction between corresponding the monomers **M1** + **M3** and **M2** + **M4,** respectively, under microwave conditions. The detailed synthesis procedures are given in ESI†. The new copolymers showed good solubility in common organic solvents used for PSCs device fabrication, such as chloroform, toluene, and chlorobenzene (CB). Initially, **P2** having 2-hexyldecyl side chains on the BT-Est was synthesized, since it is well known that the variation of alkyl side chain length and position affect the optoelectronic properties, crystallinity, and PSC performances in conjugated polymers [27,45]. However, because of its poor solubility, a longer alkyl chain (2-decyltetradecyl) was introduced. The number-average molecular weights (M_n) of **P1** and **P2** were 61.9 and 45.6 kDa, respectively, and their polydispersity indices (PDI) were 1.79 and 2.13, respectively; estimated using gel-permeation chromatography (GPC) against polystyrene standards. Both **P1** and **P2** displayed good thermal stability, with decomposition temperatures (T_d) above 330 °C (at 5% weight loss) at a heating rate of 10 °C/min; the values of T_d were evaluated by thermogravimetric analysis (TGA) in a nitrogen atmosphere (Table 1 and Fig. S1, ESI†).

The UV–vis spectra of the polymers are shown in Fig. 2, and the related optical data are summarized in Table 1. The BT-Est polymers displayed typical dual absorption bands, with the main absorption region ranging from 300 to 700 nm, complementary to non-fullerene acceptor 3,9-bis(2-methylene-(3-(1,1-dicyanomethylene)-indanone))-5,5,11,11-tetrakis(4-hexylphenyl)-dithieno[2,3-*d*:2′,3′-*d*′]-*s*-indaceno [1,2-*b*:5,6-*b*′]dithiophene (ITIC); which would allow them to harvest more photons in PSCs. The first band around 300–400 nm in Fig. 2a and b is ascribed to the localized π–π* transitions in the conjugated backbone, while the second band corresponds to the intramolecular charge transfer from a donor BDT unit to the BT-Est acceptor [46]. Compared to solutions, the absorption spectra of **P1** and **P2** in the thin-film state displayed ~20–40 nm red-shifts, attributed to the enhanced planarity and interchain π-π stacking of polymers [22,29]. Moreover, **P1** exhibited an absorption spectrum that is ~20 nm wider than that of **P2** due to the stronger interchain interaction introduced by the shorter alkyl side chains in the polymer backbone [47]. However, there was no prominent vibrionic peak was observed in either of the polymers in the thin-film state. This indicating that the carboxylate group on BT has a negative effect on the polymer packing in the solid state. Using the Beer–Lambert law ($A = \varepsilon bc$), the molar absorptivity coefficients (ε) of **P1** and **P2** were calculated to be 42485 and 34058 $M^{-1}\,cm^{-1}$, respectively (Fig. 2a). The higher ε values of **P1** would assist in light harvesting, thus boosting the J_{SC} in PSCs. The optical bandgaps of **P1** and **P2** were determined from their absorption onsets were found to be 1.67 and 1.71 eV, respectively.

The frontier energy levels of the polymers were estimated by cyclic voltammetry (CV) (Fig. 2c and d). The HOMO energy levels of **P1** and

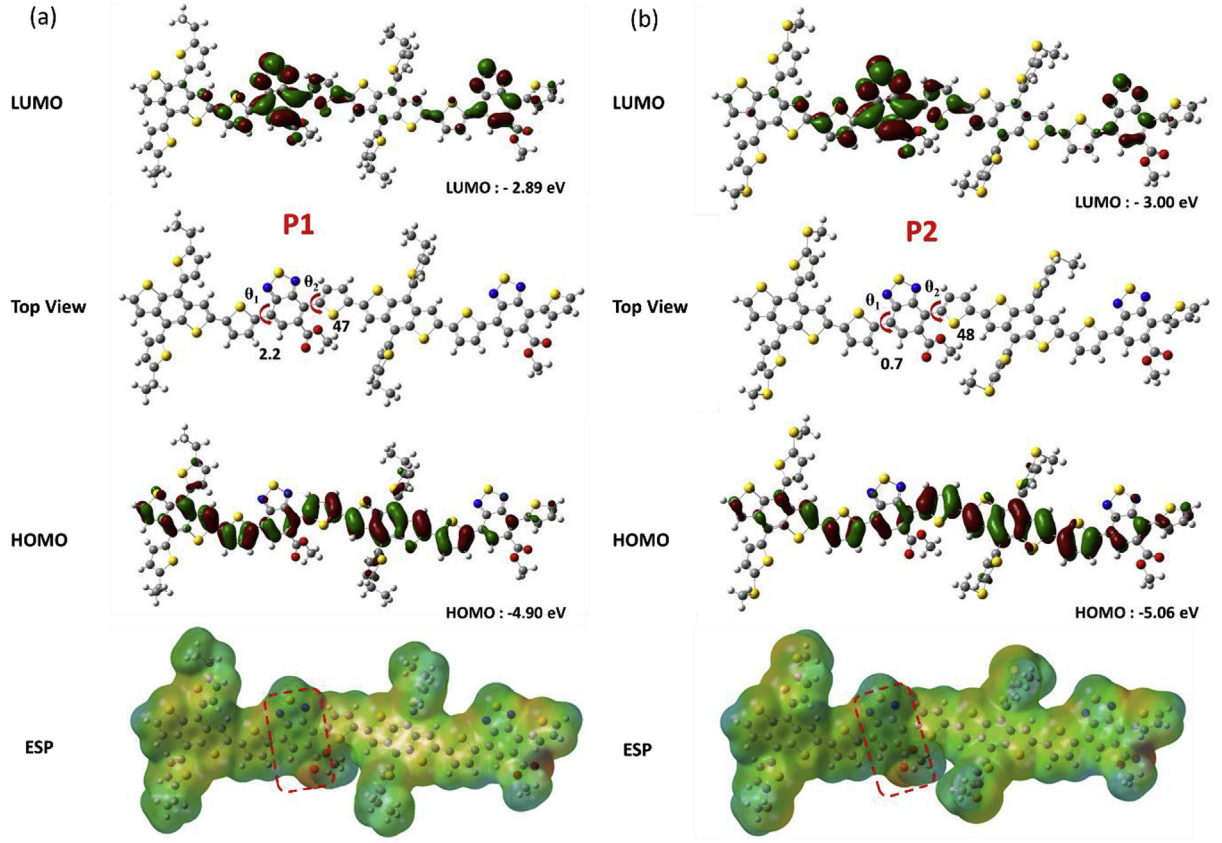

Fig. 3. Optimized geometries, isodensity surface plots, energy levels and map of electrostatic potential (ESP) surfaces of dimer model molecules of (a) **P1** and (b) **P2** polymers, calculated using the Gaussian 09 package at the B3LYP/6–31G* level.

P2 were determined to be −5.48 and −5.54 eV, respectively, from their onset oxidation potential (E_{ox}) by using the equation HOMO = −(E_{ox} + 4.8) (eV) [48]. The corresponding LUMO levels were found to be −3.81 and −3.83 eV by subtracting HOMO from the optical bandgap of polymers in the thin-film state (E_g^{opt}), i.e., LUMO = E_g^{opt} − HOMO. Thus, both HOMO and LUMO energy levels in the polymers were effectively lowered due to the increased electron affinity of the BT-Est. At the same time, the frontier energy levels of **P2** were further lowered compared to **P1**. This change is ascribed to the combined effects of (a) the steric factor, ascribed to the higher-branched chain hindering planarization and compact π-stacking in the polymer backbone [27,47] and (b) the electronic factor, arising from the thioalkyl side chains acting as π-electron acceptors and reducing the electron-donating ability of the BDT unit [49,50]. As the open-circuit voltage (V_{OC}) in PSC is directly proportional to the energy offset between the polymer donor's HOMO and the polymer acceptor's LUMO, both polymers could yield higher V_{OC} in the corresponding PSCs owing to their lower HOMO energy levels.

Theoretical calculations for the structures of **P1** and **P2** were performed using DFT to further understand the impact of the new BT-Est acceptor on the molecular orientation and energy levels of the polymers (Fig. 3). To simplify the computation, alkyl chains were minimized to methyl chains, and calculations based on two repeating monomers were performed. Notably, in Fig. 3, there was no steric hindrance was observed between the BDT units and the adjacent thiophene for both polymers (the dihedral angle, θ_1, was found to be 2.2° and 0.7°, respectively, for **P1** and **P2**). In contrast, a prominent dihedral angle, θ_2, of ~48° was observed between the BT-Est unit and the adjacent thiophene (next to the carboxylate substitution), which resulted from the steric effect of the carboxylate group on the BT unit. The dihedral angles between the **P1** and P(BT2Est-BDT) structures were also estimated to understand the effect of the number of carboxylate substituents on the BT units (Fig. S2, ESI†). Thus, limiting one carboxylate substituent on BT significantly reduced the steric repulsion between BDT and the adjacent thiophene unit when compared to their BT-2Est counterparts (θ_1 = 2.2° and 48.2°, respectively, for **P1** and P(BT2Est-BDT)). In both **P1** and **P2**, the HOMO energy levels were delocalized over BDT and the adjacent thiophene, while the LUMO energy levels were concentrated on the BT-Est acceptor. These HOMO–LUMO energy level trends were in good agreement with experimental CV results, as shown in Table 1. The electrostatic potential (ESP) surface images of both the polymers demonstrated identical potential along the backbone, expect strong electron withdrawing carboxylate group on the BT-Est core which has a positive potential (highlighted in dotted line). This suggesting BT-Est has a strong accepting nature. Consequently, the DFT results indicate that well-defined D–A type structures were formed in the conjugated backbone, which could facilitate effective π-electron delocalization for intramolecular charge transfer.

To evaluate the effect of the new BT-Est acceptors on the photovoltaic performances of the polymers, PSCs with an inverted configuration (indium–tin oxide (ITO)/zinc oxide (ZnO)/active layer/MoO_3/Ag) were fabricated. The non-fullerene acceptor ITIC was used as the acceptor unit to test the efficiency of the polymers for the following reasons. First, the energy levels of both polymers are better matched with ITIC than with $PC_{71}BM$, which can yield efficient charge separation in PSCs. Second, ITIC exhibits absorption that is complementary to that of **P1** and **P2**, which would boost J_{SC} by utilizing the broad absorption spectrum. Therefore, BT-Est based polymers are expected to show good compatibility with the ITIC acceptor. At the beginning of the evaluation, the blend ratio of the polymer–ITIC system, spin-coating speed, solvent additive, and other parameters were optimized to maximize the efficiency. Fig. 4 show the current-density versus voltage (*J*–*V*) and external quantum efficiency (EQE) plots of the optimized devices, and the corresponding photovoltaic results are summarized in

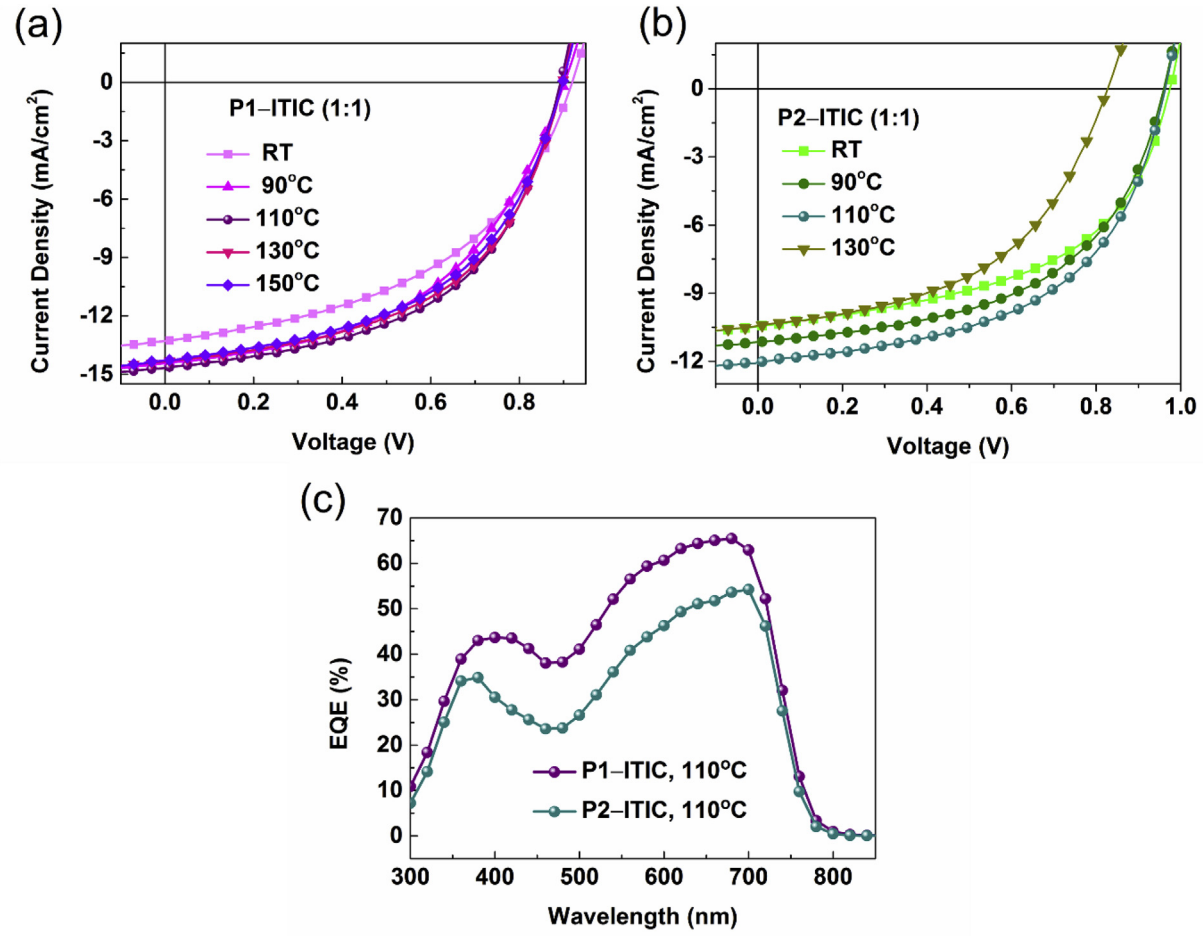

Fig. 4. J–V curves of devices with inverted configurations based on (a) P1–ITIC (1:1), (b) P2–ITIC (1:1) prepared with different annealing temperatures and processed in a solution of CB and 0.5 vol% DIO. and, (c) corresponding EQE profiles of the best devices.

Table 2
Photovoltaic performance of polymer–ITIC (1:1) devices processed in CB with 0.5 vol% DIO under AM 1.5G illumination at 100 mW cm^{-2}.

Polymer	Annealing temperature [°C]	V_{OC} [V][a]	J_{SC} [mA cm^{-2}][a]	FF [%][a]	PCE[a] [%]	μ_h [cm^2 V^{-1} s^{-1}][b]
P1	–	0.92 (0.90 ± 0.02)	13.3 (13.1 ± 0.2)	47.2 (47.8 ± 0.7)	5.8 (5.6)	5.99×10^{-5}
	90	0.90 (0.88 ± 0.02)	14.5 (14.2 ± 0.3)	48.9 (48.1 ± 0.8)	6.4 (6.2)	
	110	0.90 (0.90)	14.6 (14.5 ± 0.1)	52.5 (51.9 ± 0.6)	6.9 (6.7)	
	130	0.90 (0.89 ± 0.01)	14.4 (14.3 ± 0.1)	51.9 (52.4 ± 0.3)	6.7 (6.6)	
	150	0.90 (0.88 ± 0.02)	14.3 (14.5 ± 0.3)	50.6 (51.1 ± 0.4)	6.5 (6.4)	
P2	–	0.98 (0.98)	10.5 (10.1 ± 0.4)	51.4 (50.8 ± 0.6)	5.3 (5.0)	3.74×10^{-5}
	90	0.96 (0.95 ± 0.01)	11.2 (10.9 ± 0.3)	52.9 (52.2 ± 0.7)	5.7 (5.4)	
	110	0.96 (0.95 ± 0.01)	12.1 (11.4 ± 0.7)	53.1 (53.0 ± 0.1)	6.2 (5.9)	
	130	0.80 (0.80 ± 0.02)	10.5 (10.2 ± 0.3)	49.6 (49.4 ± 0.2)	4.2 (4.1)	

Device architecture: ITO/ZnO/active layer/MoO_3/Ag.
[a] The average PCE in parentheses was obtained from 6 to 10 independent devices.
[b] The hole-only device had the configuration ITO/PEDOT:PSS/active layer/MoO_3/Au.

Table 2. The polymers **P1** and **P2** exhibited PCEs of 5.8% and 5.3%, respectively with the optimized active layer blend ratio of 1:1 in CB and 0.5 vol% 1,8-diiodooctane (DIO). It is evident that the strong electron-withdrawing ability of the BT-Est acceptor enabled both polymers to exhibit high V_{OC} in the range of 0.92–0.98 V. Meanwhile, **P1** showed a high J_{SC} because of its broad UV absorption and higher absorptivity. In terms of PSC engineering, a method like thermal annealing have proved to enhance PSC efficiency by improving the nanoscale bulk heterojunction (BHJ) morphology [51–53]. Thus, we employed the same technique to further improve the PCEs of our polymers. Notably, the PCEs of the polymers were substantially enhanced as the thermal annealing temperature was increased to 110 °C, while temperatures above 110 °C had a negative effect (Fig. 4a and b; Table 1). The **P1** devices thermally annealed at 110 °C for 10 min exhibited the best PCE of 6.9%, with a significantly higher J_{SC} of 14.6 mA cm^{-2}, fill factor (FF) of 52.5%, and a slightly lower V_{OC} of 0.9 V (average PCE was 6.7% for over 10 devices). The Likewise, the PCE of the **P2** devices was also improved from 5.3% to 6.2% (J_{SC} = 12.44 mA cm^{-2}, FF = 53.1%, and V_{OC} = 0.96 V) after thermal annealing. Details of the optimization of the polymers are provided in Figs. S3, S4 (ESI†) and Table S2, S3 (ESI†). The improvement in the PCEs was primarily due to improved J_{SC} and FF, which indicate thermal annealing benefits the optimal phase-separated BHJ morphology and effective charge transport between the active layer and the electrode [51]. Furthermore, the V_{OC} of the **P2**

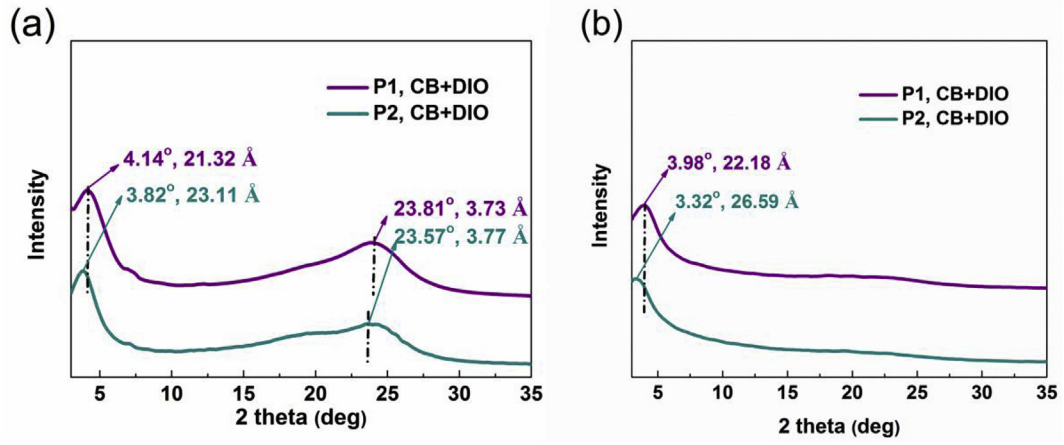

Fig. 5. (a) Out-of-plane and (b) in-plane profiles of the XRD patterns obtained from pristine polymers **P1** and **P2**.

devices decreased dramatically to 0.80 V after thermal annealing at 130 °C. These results were attributed to the poor thermal stability and intramolecular π-π stacking of **P2** introduced by 2-decyl tetradecyl alkyl chains in polymer backbone (can be seen clearly in TGA and XRD images), which also negatively affected morphological stability **P2**:ITIC blend films in PSCs.

The EQE profiles of the best PSCs were compared to understand the J_{SC} variations in **P1** and **P2** (Fig. 4c). The calculated current from the EQE curve was in good agreement (within 5% error) with the value of J_{SC} obtained from *J–V* measurements. The **P1**–ITIC device showed a broad spectral response, with absorption in the 400–750 nm range and maximum EQE reaching 65% at 675 nm, signifying that the complementary absorption of both **P1** and ITIC facilitated effective light harvesting. In contrast, the **P2**–ITIC device displayed a much poorer EQE response over the entire spectrum, indicating poor photocurrent generation [15]. These results are well-matched with the absorbance spectra and the absorption coefficients of the polymers.

As high and balanced charge-carrier mobility will determine the PCE of the PSCs, we estimated the hole mobility (μ_h) and electron mobility (μ_e) of the polymer–ITIC blend films using the space-charge-limited current (SCLC) method. Hole-only and electron-only devices were fabricated under optimal device fabrication conditions to estimate the charge-carrier mobilities; the corresponding device structures and their results are listed in Fig. S5 (ESI†). The hole and electron mobilities values were found to be 5.99×10^{-5} and 7.73×10^{-5} $cm^2 V^{-1} s^{-1}$ ($\mu_h/\mu_e = 0.77$) for **P1** and 3.74×10^{-5} and 7.42×10^{-5} $cm^2 V^{-1} s^{-1}$ ($\mu_h/\mu_e = 0.50$) for **P2**. The **P1** showed slightly higher hole mobility than **P2**, possibly because of its higher molecular weight and shorter alkyl chains, which favoured effective intermolecular interaction in the polymer backbone [54]. As reported in previous works, high charge mobility can minimize charge-recombination, thereby boosting the current densities and performances of the photovoltaic devices [55]. Thus, owing to its broader EQE, higher and more balance balanced charge mobility, PSCs employing **P1** exhibited higher J_{SC} and PCE.

To gain a clear understanding of the molecular ordering in the BT-Est based polymers, X-ray diffraction (XRD) of the pristine polymers were measured. Fig. 5a and b represent the related out-of-plane (OOP) and in-plane (IP) profiles, respectively of the BT-Est polymers. The XRD patterns of the neat polymer films exhibit prominent lamellar (100) peaks in both OOP and IP directions, with corresponding d-spacings of 21.32 and 22.18 Å, respectively, for **P1** and 23.11 and 26.59 Å, respectively, for **P2**. They also exhibit (010) peaks along the OOP direction at $2\theta = 23.81$ and 25.57°, which correspond to π–π stacking distances of 3.73 and 3.77 Å, respectively, for **P1** and **P2**. These results suggest the coexistence of edge-on and face-on crystallites in both pristine **P1** and **P2** films. Moreover, when compared to **P2**, **P1** displayed shorter distances in both the OOP and IP directions because of its shorter alkyl chains. Several studies already emphasized that the shorter π–π stacking distance between polymers will facilitate charge transport by decreasing the energy barrier for charge hopping [56]. Thus, **P1** exhibited higher crystallinity, which could facilitate effective π-electron transport and charge-carrier mobility [16,29]. These results are in good agreement with the high charge-carrier mobility and J_{SC} values observed for the **P1**–ITIC blend films.

Finally, the BHJ morphology, charge transfer, and exciton-dissociation behavior of the polymer–ITIC blends were studied using atomic force microscopy (AFM) and photoluminescence (PL) spectra to examine their effects on the variation of the photocurrent in the polymers (Fig. 6). It is well known that a smooth BHJ morphology combined with a homogeneous intermixed blend will lead to a larger D–A interface area, thus facilitating efficient exciton dissociation and transport [16,55]. In the AFM height images, the blend films of both polymers showed nearly flat and smooth morphology, but there was aggregation of distinct polymer and ITIC phases in **P2** (Fig. 6a and b). These macrophase separations adversely limit the efficient exciton dissociation by lowering donor/acceptor interfacial area and thereby leading to lower *Jsc*, FF and PCEs. Meanwhile, **P1** blend film exhibits higher root-mean-square (RMS) roughness (0.98 nm) than **P2** blend (RMS roughness = 0.78 nm), indicating the higher crystallinity of **P1** which well-matched with the crystallinity of the polymer as discussed in XRD studies (Fig. 5). The higher roughness will further reduce the internal resistance and facilitate light absorption via higher light scattering, thereby boosting J_{SC} and PCE of the PSC as reported previously [57]. To further substantiate these observations, PL quenching data of the polymer blends were measured as shown in Fig. 6e–h. The pristine **P1** and **P2** films showed PL peaks around 620–900 nm, whereas ITIC showed peaks around 720–900 nm. However, after mixing with ITIC, this PL emission was quenched by about 84.5 and 70%, respectively, for polymers **P1** and **P2** under optimized device-fabrication conditions (Fig. 6e and f). This emphasizes the better electron transfer between the **P1** and ITIC [16,29]. Similarly, both the blend films were also excited at 700 nm to quantify the effective hole transfer to the polymer (Fig. 6g and h). Noticeably, the emission was quenched by 90 and 86% for the **P1**–ITIC and **P2**–ITIC blend films, respectively. Consequently, the **P1**–ITIC blend film has efficient exciton-dissociation and charge-transport with lower recombination, which benefitting overall J_{SC} and PCE in the PSCs [58]. These results agree with morphology and photovoltaic results. Thus, the major factors that boosted the J_{SC} values of the **P1**–ITIC blend were determined to be broad absorption, high absorption coefficient, high charge-carrier mobility, and effective exciton dissociation.

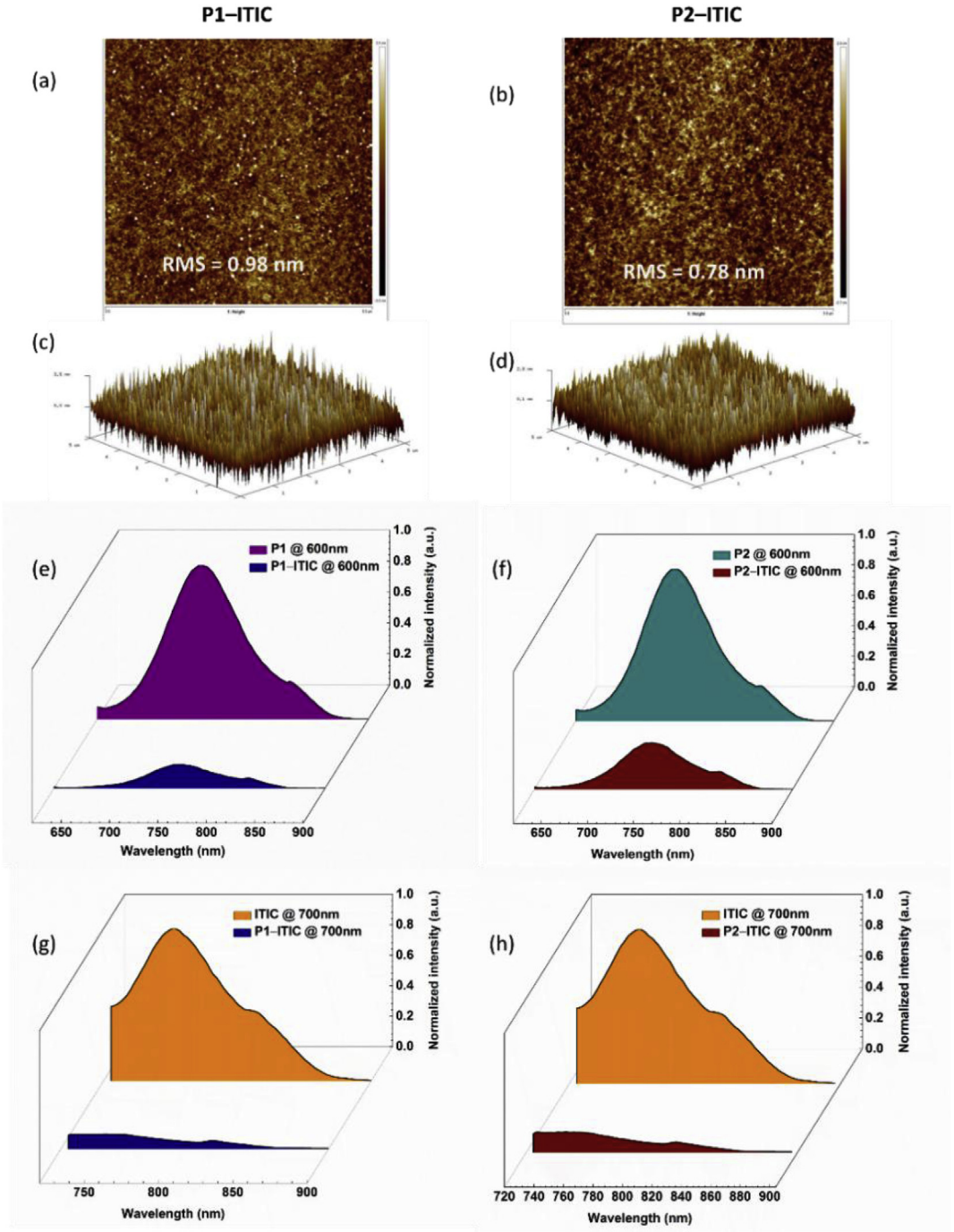

Fig. 6. AFM height (top) and three-dimensional topography images (bottom) of the (a, c) **P1**–ITIC and (b, d) **P2**–ITIC and (e–h) photoluminescence spectra (PL) of polymers **P1** and **P2** (excited at 600 nm) and ITIC (excited at 700 nm) films, as well as polymer–ITIC blend films (excited at 600 and 700 nm), processed under optimized device-fabrication conditions (polymer/ITIC mixing ratio of 1:1, 110 °C, 10 min).

3. Conclusion

We synthesized a new electron-deficient acceptor core, BT-Est, by incorporating a mono alkoxy-carboxylate group at the 5-position of the thienyl-flanked benzothiadiazole unit via cyclo-addition and its donor–acceptor polymers for application in organic photovoltaics. The BT-Est polymers demonstrated broad absorption and lower frontier energy levels simultaneously owing to the introduction of the electron withdrawing carboxylate substituent to the BT unit. Moreover, the carboxylate group provided an additional alkylation site, which facilitated easy control over the solubility and intermolecular interactions in the final polymers. Among the PSCs, the device employing **P1** exhibited high absorption coefficients and hole mobility, shorter intermolecular π–π stacking distance, and effective exciton dissociation and charge transport rate, resulting in the best PCE of 6.9%, with high J_{SC}. Although the PCEs of the BT-Est based PSCs were moderate compared to current high-PCE non-fullerene solar cells, there remains substantial scope for further improvement of PCEs by improving the FF and J_{SC}. Further tests such as optimization of polymer design by employing more appropriate donor units, tuning alkyl chains to enhance J_{SC} and device engineering like modifying hole and/or electron layers, optimizing BHJ morphology by methods such as using more appropriate solvent additives and solvent vapor annealing to improve the FF of these PSCs are underway. Our results demonstrate that new BT-Est

acceptor can be used for synthesizing versatile D–A conjugated polymers and small molecules for organic electronic applications.

Acknowledgements

This research was supported by the New & Renewable Energy Core Technology Program (No. 20153010140030) and Human Resources program in Energy Technology (No. 20174010201540) of the Korea Institute of Energy Technology Evaluation and Planning (KETEP) grant funded by the Ministry of Trade, Industry & Energy, Republic of Korea. This research was supported by the 2018 KU Brain Pool of Konkuk University.

Appendix A. Supplementary data

Supplementary data related to this article can be found at https://doi.org/10.1016/j.dyepig.2018.12.058.

References

[1] Wang Y, Michinobu T. Benzothiadiazole and its π-extended, heteroannulated derivatives: useful acceptor building blocks for high-performance donor–acceptor polymers in organic electronics. J Mater Chem C 2016;4:6200–14.
[2] Zhou H, Yang L, Stuart AC, Prince SC, Liu S, You W. Development of fluorinated benzothiadiazole as a structural unit for a polymer solar cell of 7 % efficiency. Angew Chem Int Ed 2011;50:2995–8.
[3] Fu B, Baltazar J, Hu Z, Chien A-T, Kumar S, Henderson CL, Collard DM, Reichmanis E. Low band gap donor–acceptor benzothiadiazole-oligothiophene based polymeric semiconductors. Chem Mater 2012;24:4123–33.
[4] Liu Y, Zhao J, Li Z, Mu C, Ma W, Hu H, Jiang K, Lin H, Ade H, Yan H. Aggregation and morphology control enables multiple cases of high-efficiency polymer solar cells. Nat Commun 2014;5:5293.
[5] Jian F, Yuen JD, Mingfeng W, Jason S, Jung-Hwa S, Reza MA, Dante Z, Alan H, Fred W. High-performance ambipolar transistors and inverters from an ultralow bandgap polymer. Adv Mater 2012;24:2186–90.
[6] Zhang C, Chen Z, Zeng W, Yu G, Yang C. Narrow band-gap copolymers with two acceptors of benzo[1,2-c;3,4-c′]bis[1,2,5]thiadiazole and benzo[c][1,2,5] thiadiazole: synthesis, characteristics and application in field-effect transistors. Dyes Pigments 2016;130:291–7.
[7] Wang Y, Nakano M, Michinobu T, Kiyota Y, Mori T, Takimiya K. Naphthodithiophenediimide–benzobisthiadiazole-based polymers: versatile n-type materials for field-effect transistors and thermoelectric devices. Macromolecules 2017;50:857–64.
[8] Wang M, Hu X, Liu P, Li W, Gong X, Huang F, Cao Y. Donor–acceptor conjugated polymer based on naphtho[1,2-c:5,6-c]bis[1,2,5]thiadiazole for high-performance. J Am Chem Soc 2011;133:9638–41.
[9] Shreyam C, Yutaka I, Makoto K, Yoshio A. Naphtho[1,2-c:5,6-c′]bis[1,2,5]thiadiazole-containing π-conjugated compound: nonfullerene electron acceptor for organic photovoltaics. Adv Funct Mater 2016;26:1161–8.
[10] Yaocheng J, Zhiming C, Sheng D, Nannan Z, Lei Y, Xiao-Fang J, Feng L, Fei H, Yong C. A novel naphtho[1,2-c:5,6-c′]bis([1,2,5]thiadiazole)-based narrow-bandgap π-conjugated polymer with power conversion efficiency over 10%. Adv Mater 2016;28:9811–8.
[11] Kawashima K, Fukuhara T, Suda Y, Suzuki Y, Koganezawa T, Yoshida H, Ohkita H, Osaka I, Takimiya K. Implication of fluorine atom on electronic properties, ordering structures, and photovoltaic performance in naphthobisthiadiazole-based semiconducting polymers. J Am Chem Soc 2016;138:10265–75.
[12] Mei C-Y, Liang L, Zhao F-G, Wang J-T, Yu L-F, Li Y-X, Li W-S. A family of donor–acceptor photovoltaic polymers with fused 4,7-dithienyl-2,1,3-benzothiadiazole units: effect of structural fusion and side chains. Macromolecules 2013;46:7920–31.
[13] Jun H, Yongxiang Z, Junwu C, Lianjie Z, Junbiao P, Yong C. Dithienobenzothiadiazole-based conjugated polymer: processing solvent-relied interchain aggregation and device performances in field-effect transistors and polymer solar cells. Macromol Rapid Commun 2014;35:1960–7.
[14] Lee J, Sin DH, Clement JA, Kulshreshtha C, Kim HG, Song E, Shin J, Hwang H, Cho K. Medium-bandgap conjugated polymers containing fused dithienobenzochalcogenadiazoles: chalcogen atom effects on organic photovoltaics. Macromolecules 2016;49:9358–70.
[15] Mori H, Nishinaga S, Takahashi R, Nishihara Y. Alkoxy-substituted anthra[1,2-c:5,6-c′]bis([1,2,5]thiadiazole) (atz): a new electron-acceptor unit in the semiconducting polymers for organic electronics. Macromolecules 2018;51:5473–84.
[16] Nguyen TL, Choi H, Ko SJ, Uddin MA, Walker B, Yum S, Jeong JE, Yun MH, Shin TJ, Hwang S, Kim JY, Woo HY. Semi-crystalline photovoltaic polymers with efficiency exceeding 9% in a ~300 nm thick conventional single-cell device. Energy Environ Sci 2014;7:3040–51.
[17] Kasey A, Dimitrov SD, Shakya-Tuladhar P, Fei Z, Nguyen M, Han Y, Anthopoulos TD, Durrant JR, Heeney M. Effect of systematically tuning conjugated donor polymer lowest unoccupied molecular orbital levels via cyano substitution on organic photovoltaic device performance. Chem Mater 2016;28:5110–20.
[18] Hu Z, Chen H, Qu J, Zhong X, Chao P, Xie M, Lu W, Liu A, Tian L, Su Y-A, Chen W, He F. Design and synthesis of chlorinated benzothiadiazole-based polymers for efficient solar energy conversion. ACS Energy Lett 2017;2:753–8.
[19] Mo D, Wang H, Chen H, Qu S, Chao P, Yang Z, Tian L, Su Y-A, Gao Y, Yang B, Chen W, He F. Chlorination of low-band-gap polymers: toward high-performance polymer solar cells. Chem Mater 2017;29:2819–30.
[20] Zhang Y, Ren F, Li Q, Zhang Z, He X, Chen Z, Shi J, Tu G. Performance comparison of fluorinated and chlorinated donor–acceptor copolymers for polymer solar cells. J Mater Chem C 2018;6:4658–62.
[21] Kim I-B, Jang S-Y, Kim Y-A, Kang R, Kim I-S, Ko D-K, Kim D-Y. The effect of fluorine substitution on the molecular interactions and performance in polymer solar cells. ACS Appl Mater Interfaces 2017;9:24011–9.
[22] Kini GP, Choi JY, Jeon SJ, Suh IS, Moon DK. Controlling the interchain packing and photovoltaic properties via fluorine substitution in terpolymers based on benzo[1,2-c:4,5-c′]dithiophene-4,8-dione and benzothiadiazole units. Polymer 2018;148:330–8.
[23] Zhao J, Li Y, Yang G, Jiang K, Lin H, Ade H, Ma W, Yan H. Efficient organic solar cells processed from hydrocarbon solvents. Nat Energy 2016;1:15027.
[24] Lee HS, Song HG, Jung H, Kim MH, Cho C, Lee J-Y, Park S, Son HJ, Yun H-J, Kwon S-K, Kim Y-H, Kim B. Effects of backbone planarity and tightly packed alkyl chains in the donor−acceptor polymers for high photostability. Macromolecules 2016;49:7844–56.
[25] Yuan J, Ford MJ, Zhang Y, Dong H, Li Z, Li Y, Nguyen T-Q, Bazan GC, Ma W. Toward thermal stable and high photovoltaic efficiency ternary conjugated copolymers: influence of backbone fluorination and regioselectivity. Chem Mater 2017;29:1758–68.
[26] Lee W, Kim G-H, Ko S-J, Yum S, Hwang S, Cho S, Shin Y-H, Kim JY, Woo HY. Semicrystalline d–a copolymers with different chain curvature for applications in polymer optoelectronic devices. Macromolecules 2014;47:1604–12.
[27] Kini GP, Lee SK, Shin WS, Moon SJ, Song CE, Lee JC. Achieving a solar power conversion efficiency exceeding 9% by modifying the structure of a simple, inexpensive and highly scalable polymer. J Mater Chem A 2016;4:18585–97.
[28] Ko S-J, Hoang QV, Song CE, Uddin MA, Lim E, Park SY, Lee BH, Song S, Moon S-J, Hwang S, Morin P-O, Leclerc M, Su GM, Chabinyc ML, Woo HY, Shin WS, Kim JY. High-efficiency photovoltaic cells with wide optical band gap polymers based on fluorinated phenylene-alkoxybenzothiadiazole. Energy Environ Sci 2017;10:1443–55.
[29] Kini GP, Hoang QV, Song CE, Lee SK, Shin WS, So WW, Uddin MA, Woo HY, Lee JC. Thiophene-benzothiadiazole based D-A(1)-D-A(2) type alternating copolymers for polymer solar cells. Polym Chem 2017;8:3622–31.
[30] Po R, Roncali J. Beyond efficiency: scalability of molecular donor materials for organic photovoltaics. J Mater Chem C 2016;4:3677–85.
[31] Liu D, Yang B, Jang B, Xu B, Zhang S, He C, Woo HY, Hou J. Molecular design of a wide-band-gap conjugated polymer for efficient fullerene-free polymer solar cells. Energy Environ Sci 2017;10:546–51.
[32] Park GE, Choi S, Park SY, Lee DH, Cho MJ, Choi DH. Eco-friendly solvent-processed fullerene-free polymer solar cells with over 9.7% efficiency and long-term performance stability. Adv Energy Mater 2017;7:1700566.
[33] Huifeng Y, Runnan Y, Joo ST, Hao Z, Shaoqing Z, Bomee J, Afsar UM, Young WH, Jianhui H. A wide bandgap polymer with strong π–π interaction for efficient fullerene-free polymer solar cells. Adv Energy Mater 2016;6:1600742.
[34] Liu Y, Zhao W, Wu Y, Zhang J, Li G, Li W, Ma W, Hou J, Bo Z. Enhancing the power conversion efficiency of polymer solar cells to 9.26% by a synergistic effect of fluoro and carboxylate substitution. J Mater Chem A 2016;4:8097–104.
[35] Yunpeng Q, Afsar UM, Yu C, Bomee J, Kang Z, Zhong Z, Runnan Y, Joo ST, Young WH, Jianhui H. Highly efficient fullerene-free polymer solar cells fabricated with polythiophene derivative. Adv Mater 2016;28:9416–22.
[36] Yang G, Liu J, Ma L-K, Chen S, Lai JYL, Ma W, Yan H. Understanding the influence of carboxylate substitution on the property of high-performance donor polymers in non-fullerene organic solar cells. Mater Chem Front 2018;2:1360–5.
[37] Park J, Ha J-W, Kim HS, Hwang D-H. Synthesis and characterization of a donor-acceptor type copolymer containing ester-functionalized benzo[c][1,2,5]thiadiazole as an accepting building block for organic photovoltaics. Thin Solid Films 2018;663:56–61.
[38] Yang Z, Chen H, Wang H, Mo D, Liu L, Chao P, Zhu Y, Liu C, Chen W, He F. The integrated adjustment of chlorine substitution and two-dimensional side chain of low band gap polymers in organic solar cells Polym. Chem 2018;9:940–7.
[39] Takacs CJ, Sun Y, Welch GC, Perez LA, Liu X, Wen W, Bazan GC, Heeger A. Solar Cell Efficiency, Self-Assembly, and dipole-dipole interactions of isomorphic narrow-band-gap molecules. J Am Chem Soc 2012;134:16597–606.
[40] Leblebici SY, Chen TL, Olalde-Velasco P, Yang W, Ma B. Reducing exciton binding energy by increasing thin film permittivity: an effective approach to enhance exciton separation efficiency in organic solar cells. ACS Appl Mater Interfaces 2013;5:10105–10.
[41] De Gier HD, Jahani F, Broer R, Hummelen JC, Havenith RWA. Promising Strategy to improve charge separation in organic photovoltaics: installing permanent dipoles in PCBM analogues. J Phys Chem A 2016;120:4664–71.
[42] Ruiz Delgado MC, Hernández V, López Navarrete JT, Tanaka S, Yamashita Y. Combined spectroscopic and theoretical study of narrow band gap heterocyclic co-oligomers containing alternating aromatic donor and o-quinoid acceptor units. J Phys Chem B 2004;108:2516–26.
[43] Hong NJ, Park H, Baek M-J, Lee S-H, Jeong J, Park JH, Zong K. Synthesis and correlation between structure and photovoltaic performance of two-dimensional BDT-TPD polymers. Org Electron 2016;35:101–11.
[44] Tao L, Xuexue P, Xiangyi M, Yu L, Donghui W, Wei M, Lijun H, Xiaobo S, Ho LT, Minjuan H, Hyosung C, Young KJ, C.W.C.H., Yanming S. Alkyl side-chain

engineering in wide-bandgap copolymers leading to power conversion efficiencies over 10%. Adv Mater 2017;29:1604251.
[45] Mei J, Bao Z. Side chain engineering in solution-processable conjugated polymers. Chem Mater 2014;26:604–15.
[46] Song CE, Kim YJ, Suranagi SR, Kini GP, Park S, Lee SK, Shin WS, Moon SJ, Kang IN, Park CE, Lee JC. Impact of the crystalline packing structures on charge transport and recombination via alkyl chain tunability of dpp-based small molecules in bulk heterojunction solar cells. ACS Appl Mater Interfaces 2016;8:12940–50.
[47] Jiang X, Yang Y, Zhu J, Lau T-K, Cheng P, Lu X, Zhan X, Chen X. Constructing D–A copolymers based on thiophene-fused benzotriazole units containing different alkyl side-chains for non-fullerene polymer solar cells. J Mater Chem C 2017;5:8179–86.
[48] Mahmood K, Lu H, Liu Z-P, Li C, Lu Z, Liu X, Fang T, Peng Q, Li G, Li L, Bo Z. Engineering the band gap and energy level of conjugated polymers using a second acceptor unit. Polym Chem 2014;5:5037–45.
[49] Yao H, Zhang H, Ye L, Zhao W, Zhang S, Hou J. Dialkylthio substitution: an effective method to modulate the molecular energy levels of 2d-bdt photovoltaic polymers. ACS Appl Mater Interfaces 2016;8:3575–83.
[50] Wang Q, Zhang S, Xu B, Li S, Yang B, Yuan W, Hou J. Efficient fullerene-free polymer solar cells based on alkylthio substituted conjugated polymers. J Phys Chem C 2017;121:4825–33.
[51] Ma W, Yang C, Gong X, Lee K, Heeger AG. Thermally Stable, Efficient polymer solar cells with nanoscale control of the interpenetrating network morphology. Adv Funct Mater 2005;15:1617–22.
[52] Gao Y, Zhu R, Wang Z, Guo F, Wei Z, Yang Y, Zhao L, Zhang Y. An asymmetrical polymer based on thieno[2,3-f]benzofuran for efficient fullerene-free polymer solar cells. ACS Appl Mater Interfaces 2018;1:1888–92.
[53] Li S, Liu W, Shi M, Mai J, Lau T-K, Wan J, Lu X, Li C-Z, Chen H. A spirobifluorene and diketopyrrolopyrrole moieties based non-fullerene acceptor for efficient and thermally stable polymer solar cells with high open-circuit voltage. Energy Environ Sci 2016;9:604–10.
[54] Xiao Z, Sun K, Subbiah J, Qin T, Lu S, Purushothaman B, Jones DJ, Holmes AB, Wong WWH. Effect of molecular weight on the properties and organic solar cell device performance of a donor-acceptor conjugated polymer. Polym Chem 2015;6:2312–8.
[55] Kini GP, Oh S, Abbas Z, Rasool S, Jahandar M, Song CE, Lee SK, Shin WS, So WW, Lee JC. Effects on photovoltaic performance of dialkyloxy-benzothiadiazole copolymers by varying the thienoacene donor. ACS Appl Mater Interfaces 2017;9:12617–28.
[56] Wu Q, Wang M, Qiao X, Xiong Y, Huang Y, Gao X, Li H. Thieno[3,4-c]pyrrole-4,6-dione containing copolymers for high performance field-effect transistors. Macromolecules 2013;46:3887–94.
[57] Paek S, Choi H, Jo H, Lee K, Song K, Siddiqui SA, Sharma GD, Ko J. A new unsymmetrical near-IR small molecule with squaraine chromophore for solution processed bulk heterojunction solar cells. J Mater Chem C 2015;3:7029–37.
[58] Xu S, Wang X, Feng L, He Z, Peng H, Cimrova V, Yuan J, Zhang Z-G, Li Y, Zou Y. Optimizing the conjugated side chains of quinoxaline based polymers for non-fullerene solar cells with 10.5% efficiency. J Mater Chem A 2018;6:3074–83.